Hindawi Publishing Corporation
Journal of Nanomaterials
Volume 2011, Article ID 137498, 6 pages
doi:10.1155/2011/137498

Research Article

Microstructure and Corrosion Behavior of Ni-Alloy/CrN Nanolayered Coatings

Hao-Hsiang Huang,[1] Fan-Bean Wu,[1] Jyh-Wei Lee,[2] and Li-Chun Chang[2]

[1] *Department of Materials Science and Engineering, National United University, Miaoli 36003, Taiwan*
[2] *Department of Materials Science and Engineering, Ming Chi University of Technology, Taipei 24301, Taiwan*

Correspondence should be addressed to Fan-Bean Wu, fbwu@nuu.edu.tw

Received 23 April 2010; Accepted 19 August 2010

Academic Editor: Bo Zou

The Ni-alloy/CrN nanolayered coatings, Ni-Al/CrN and Ni-P/CrN, were deposited on (100) silicon wafer and AISI 420 stainless steel substrates by dual-gun sputtering technique. The influences of the layer microstructure on corrosion behavior of the nanolayered thin films were investigated. The bilayer thickness was controlled approximately 10 nm with a total coating thickness of 1 μm. The single-layer Ni-alloy and CrN coatings deposited at 350°C were also evaluated for comparison. Through phase identification, phases of Ni-P and Ni-Al compounds were observed in the single Ni-alloy layers. On the other hand, the nanolayered Ni-P/CrN and Ni-Al/CrN coatings showed an amorphous/nanocrystalline microstructure. The precipitation of Ni-Al and Ni-P intermetallic compounds was suppressed by the nanolayered configuration of Ni-alloy/CrN coatings. Through Tafel analysis, the E_{corr} and I_{corr} values ranged from –0.64 to –0.33 V and 1.42×10^{-5} to 1.14×10^{-6} A/cm^2, respectively, were deduced for various coating assemblies. The corrosion mechanisms and related behaviors of the coatings were compared. The coatings with a nanolayered Ni-alloy/CrN configuration exhibited a superior corrosion resistance to single-layer alloy or nitride coatings.

1. Introduction

Nanolayered thin film was recognized as a coating with alternating layers of two different materials with dissimilar physical, chemical, and related characteristics. With proper control of layer composition and microstructure, multilayered coatings could yield superior mechanical properties than monolayer ones [1–5]. Chromium nitride thin films have been investigated and demonstrated to exhibit good mechanical performance, thermal properties, and antioxidation behavior [6, 7]. Also, Ni-based alloy coatings were frequently adopted as protective alloy coatings due to their various merits, including corrosion resistance, toughness, and wear resistance [8–10]. The combination of these two materials systems to form a dual layer composite coating was a possible way to further the coating properties [11–13]. Several materials systems with nanolayer configuration, such as CrN/AlN, TiN/CrN, Ag/Pd, and Au/Ag, had been developed [1, 14–16]. However, limited literature on nitride/alloy coating systems were published. The integration of CrN and Ni-alloy in a nanolayered feature was thus of great interest. Moreover, the control of the nanolayered configuration, layer microstructure, and related properties was not fully understood. In this study, Ni-P/CrN and Ni-Al/CrN nanolayered coatings were fabricated by dual-gun sputtering technique. The microstructure and phases of the multilayer coatings were controlled by process temperature during sputtering. The corrosion behavior of the multilayer coatings was investigated through electrochemical potentiodynamic analysis. The relationship between microstructure, phases, and corrosion behavior of the nanolayered Ni-P/CrN and Ni-Al/CrN coatings was discussed.

2. Experimental Details

The Ni-alloy/CrN nanolayered coatings were deposited on the silicon (100) and 420 stainless substrates by dual-gun sputtering technique. The $Ni_{70}Al_{30}$ and $Ni_{75}P_{25}$ (in at.%) sputtering targets of 50.8 mm in diameter were employed for alloy layer fabrication. The CrN coating was deposited

using a Cr target with 99.9% in purity and N_2 gas as reactive source. Before deposition, the chamber was evacuated down to 4.0×10^{-4} Pa. The high purity Ar flow was introduced to a working pressure of 2.7×10^{-1} Pa. Presputtering was performed for 10 minutes to clean the target surface followed by the fabrication process. The target powers were D.C. 100 W for Ni-alloy and R.F. 200 W for Cr. The working pressure was 2.7×10^{-1} Pa for Ni-alloy fabrication, while a working pressure of 6.7×10^{-1} Pa was adopted for CrN due to the coinlet of N_2 gas. The process temperature was fixed at 350°C for all coating assemblies. Nanolayered Ni-alloy/CrN coatings were prepared with fixed bilayer period of 10 nm. The deposition time of individual layer of multilayer Ni-alloy/CrN coatings during sequential sputtering were modified from 30 to 120 seconds. The total thickness of the multilayer coating systems was controlled around 1.0 μm. The thickness ratio of Ni-alloy and CrN was fixed at 1.0. An X-ray diffractometer (Shimadzu, XRD-6000, Japan) with continuous θ–2θ scan was used to identify the phases in the coatings. The 2θ scan ranged from 30° to 65° with a step width of 0.02° at a scanning speed of 6°/min. The microstructure and surface morphology of the coatings were evaluated by FE-SEM (JSM-6500, JEOL, Japan). The compositions of selected areas of corroded coatings were inspected by an energy dispersion spectra inspected analyzer (INCA Energy 350, Oxford, UK). The depth profile was measured by Auger electron nanoscope (PHI 700, ULVAC-PHI, Japan). The corrosion behavior was measured by an electrochemical workstation (Jiehan-5000, Jiehan, Taiwan). The corrosion test was operated in 3.5 M NaCl aqueous solution at room temperature with the saturated calomel electrode (SCE) as the reference electrode. The scanning range was from −0.25 to +0.25 V according to the open circuit potential of each sample. The potentiodyanmic curves were fitted using CorrView software. For convenience, coatings deposited on Si substrates were applied in cross-sectional SEM observation, nano-Auger analysis, and XRD phase identification. Corrosion test and related analyses were conducted on coatings deposited on stainless steel substrates.

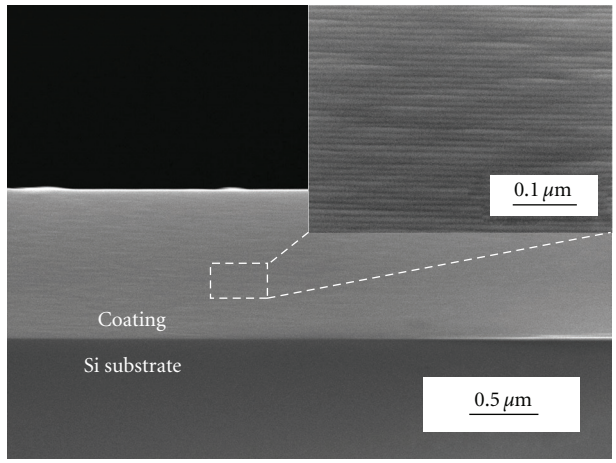

Figure 1: The cross-sectional FE-SEM images of NiP/CrN nanolayered coatings.

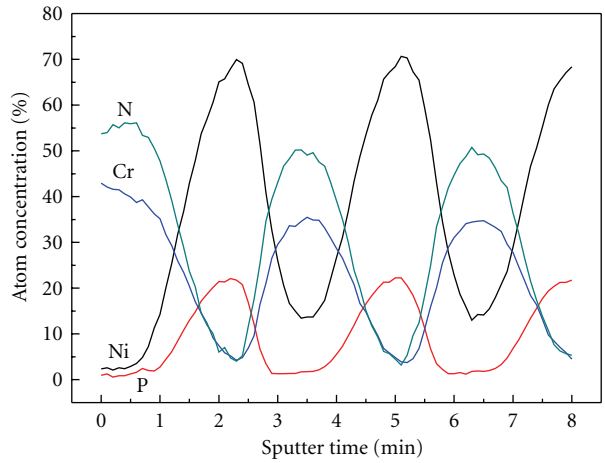

Figure 2: Nano-Auger depth analysis of NiP/CrN nanolayered coating.

3. Results and Discussion

The cross-sectional view of the Ni-P/CrN and Ni-Al/CrN nanolayered coatings was presented in Figure 1. Smooth and dense coating configurations were recognized by sputtering fabrication process. The total thickness of all coatings estimated from FE-SEM images were about 1 μm. In the magnified regions, as indicated in Figure 1, the smooth configuration of the Ni-P and CrN stacking was observed. A bilayer thickness of approximately 10 nm could be measured. To confirm the multilayer feature, the depth analysis of Ni-P/CrN nanolayered coating was conducted by nano-Auger technique. The sputter time was set to be 3 nm/min. The depth profile of Ni, P, Cr, and N showed a sequentially alternating distribution with a bilayer thickness around 10 nm, as shown in Figure 2. A nanolayered structure of the coating was again demonstrated. The X-ray patterns of single and nanolayer coatings were shown in Figure 3. The diffraction peaks of CrN (111), (200), and (220) were found for CrN coating. The Ni_3Al precipitation was identified in the single-layer Ni-Al coating, while the Ni crystalline phase and Ni_3P precipitation was discovered in the Ni-P coating. This indicated that sputtering process and substrate heating enhanced the precipitation of the Ni-P and Ni-Al coatings. It should be noted that the peaks of Ni-P and Ni-Al intermetallic compounds were not fully resolved according to their broadened peak widths. In the Ni-Al/CrN and Ni-P/CrN coatings, the diffraction peaks were further broadened that a nanocrystalline/amorphous microstructure was expected. Since the thickness of each layer was 5 nm, the precipitation of Ni-Al, Ni-P intermetallics, and CrN phases was restricted by nanolayer feature. In the Ni-Al/CrN coating, three major peaks of CrN were recognized. However, a few peaks of Ni crystallites found in single Ni-Al coating layer vanished. Similar situation was found for single Ni-P and nanolayered Ni-P/CrN coatings. It was believed that the precipitation of intermetallic compounds was suppressed by

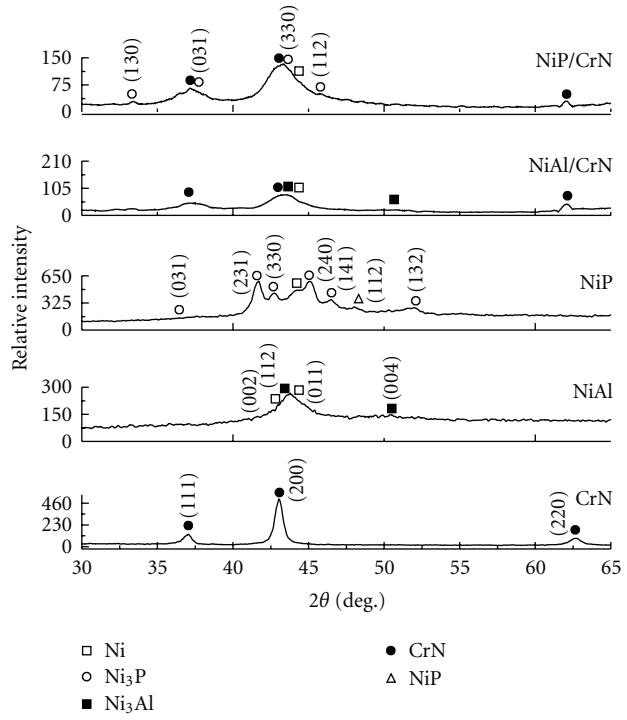

Figure 3: The XRD patterns of various coating systems.

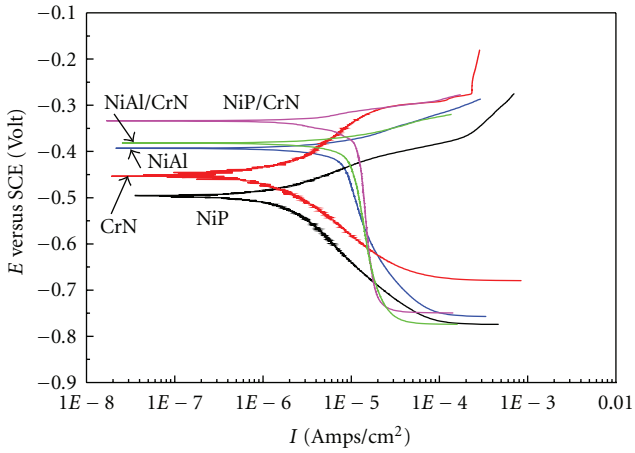

Figure 4: The electrochemical polarization curves of various coating systems.

nanolayered sequential deposition. To summarize, the Ni-Al and Ni-P single coatings exhibited precipitated structure, while nanolayered coatings showed CrN phases with Ni-alloy nanocrystalline layers.

The results of potentiodynamic analysis for various coating systems were indicated in Figure 4. The trend of corrosion resistance in different coatings systems could be discovered. The numberical results of I_{corr} and E_{corr} were listed in Table 1. The E_{corr} values were from -0.64 to -0.33 V. The I_{corr} values ranged from 1.42×10^{-5} to 1.14×10^{-6} A/cm^2. All the coatings showed better corrosion potentials than that of AISI 420 substrate. Firstly, for the

Table 1: The E_{corr} and I_{corr} values of various coating systems.

Materials	E_{corr} (V versus SCE)	I_{corr} (A/cm^2)
420 SS	-0.64	1.42×10^{-5}
NiAl	-0.39	1.20×10^{-5}
NiP	-0.50	1.34×10^{-6}
CrN	-0.45	1.14×10^{-6}
NiAl/CrN	-0.38	1.18×10^{-5}
NiP/CrN	-0.33	7.50×10^{-6}

*The test was conducted in a 3.5 M NaCl solution at room temperature.

single-layer coatings, the Ni-Al coating showed the most nonnegative E_{corr} value of -0.39 Volts. The Ni-P and Cr-N coatings exhibited the less I_{corr} values of 1.14×10^{-6} and 1.34×10^{-6}, respectively. This could be due to different corrosion behavior for the Ni-Al, Ni-P, and CrN coatings. For the Ni-Al coating, the corrosion occurred homogeneously and isotropically on coating surface [10]. On the other hand, the Ni-P and CrN showed in-depth pitting corrosion on localized areas [12, 17]. This could be referred to the corroded surface morphology of Ni-Al, Ni-P, and CrN, as shown in Figures 5(a), 5(b), and 5(c). Large but homogeneously distributed corroded areas were observed for the Ni-Al coating. On the contrary, localized small etching pits were found for Ni-P and CrN coatings, as indicated in Figures 5(b) and 5(c). Secondly, take Ni-Al, CrN, and Ni-Al/CrN coatings for comparison, the E_{corr} and I_{corr} values of these two coatings were similar. Figure 5(d) showed the surface morphology of Ni-Al/CrN coating. The pits were less than other single-layer coatings. However, the large I_{corr} of Ni-Al was not significantly decreased by nanolayered feature. Through EDX analysis, a few Fe concentration were detected in the single Ni-Al coating, indicating some of the Ni-Al was coating etched away. Nevertheless, in the Ni-Al/CrN coating, the substrate was well protected by the coating. The corrosion behavior of Ni-P, CrN, and Ni-P/CrN was also compared. The Ni-P/CrN exhibited a superior corrosion resistance than those of other thin films. It should be noted that the Ni-P coating exhibited a lowest E_{corr} value between all materials systems. The enhancement of nanolayered Ni-P/CrN as compared to CrN coating was evident. The surface morphology of Ni-P/CrN after corrosion test was shown in Figure 5(e). The etching pits were significantly reduced. The corrosion resistance was thus improved effectively for the combination of Ni-P and CrN coatings.

The corrosion behaviors of the nanolayered Ni-P/CrN and Ni-Al/CrN coatings were taken into comparison. Even the E_{corr} of Ni-P was lower than that of Ni-Al coating, as the Ni-P and Ni-Al were deposited with CrN to form nanolayered coatings, the corrosion resistance of Ni-P/CrN was better than that of Ni-Al/CrN nanolayered coating. This was because Ni-Al layer exhibited a severer layer area corrosion mechanism, while similar localized pitting corrosion was found for both Ni-P and CrN layers. Nevertheless, nanolayered coatings exhibited good protection from corrosion attacks. The corroded surface morphologies of two nanolayered coatings were shown in Figure 6. Though

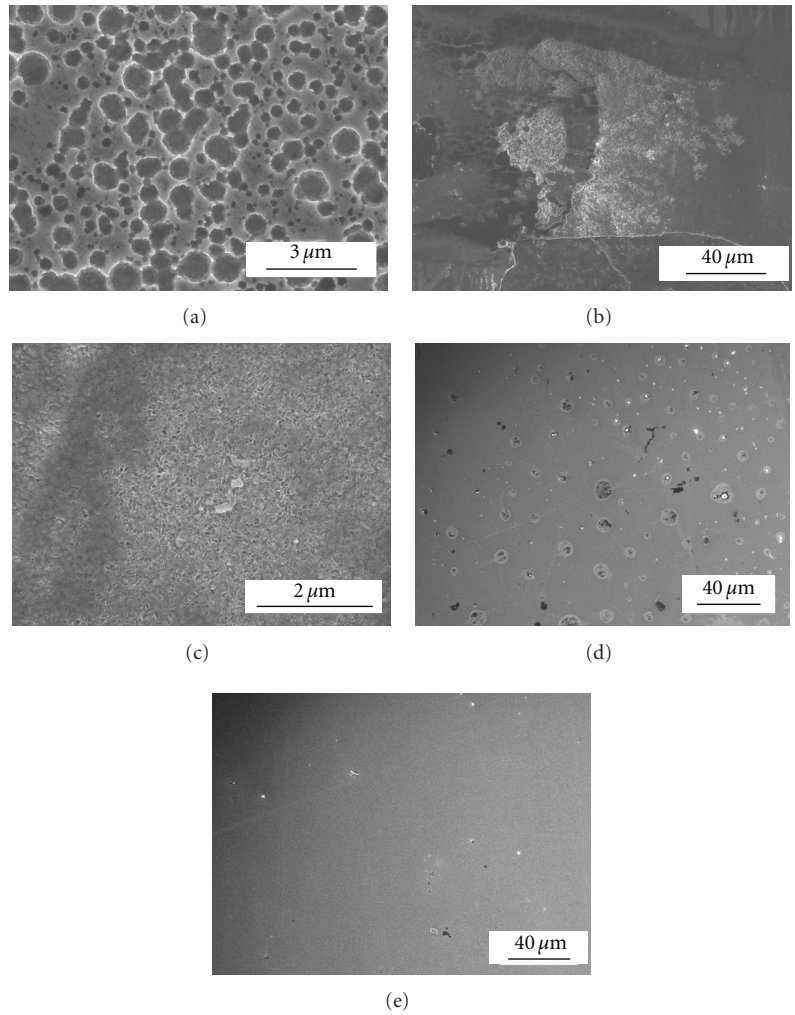

Figure 5: The SEM surface images of (a) NiAl, (b) NiP, (c) CrN, (d) NiAl/CrN nanolayered, and (e) NiP/CrN nanolayered coatings on stainless steel substrates after corrosion test.

etching pits were observed at localized area, the substrate was still well covered with coating. This phenomenon was consistent to the fitted results of potentiodynamic curves. Corrosion resistance was improved through Ni-P/CrN and Ni-Al/CrN nanolayered feature.

The corrosion mechanisms of the nanolayered coatings were shown in Figure 7. First, the corrosion resistance of Ni-Al/CrN nanolayered could be slightly improved by the nanolayer feature. Localized etching pits in CrN layers with homogenous corrosion behavior in the Ni-Al layer were expected for the Ni-Al/CrN coatings. In the Ni-P/CrN nanolayered coating, due to the pitting behavior of both Ni-P and CrN layers, the corrosion attach detoured in the interface and elongated the corrosion path. The corrosion resistance was thus improved by such configuration. To sum up, the combination of Ni-alloy and CrN to form a nanolayered coating was beneficial to corrosion protection in surface coatings. The introduction of interphase interface elongated the corrosion path and retarded the corrosion attack in the Ni-alloy/CrN nanolayered coatings.

4. Conclusions

Nanolayered Ni-alloy/CrN coatings systems were successfully fabricated by dual-gun sputtering technique. The coatings showed smooth and dense structure, as revealed in FE-SEM cross-sectional images. The Ni-P/CrN and Ni-Al/CrN nanolayered layer coatings exhibited a nanocrystalline/amorphous microstructure because of the restricted precipitation by nanolayer feature. For the single-layer coatings, Ni-Al exhibited a homogeneously large area corrosion phenomenon, while localized pitting within limited regions was found for NiP and CrN coatings. Through Tafel analysis, the Ni-alloy/CrN nanolayered coating exhibited a superior corrosion resistance than monolayer coatings. Moreover, the Ni-P/CrN coating showed an even greater corrosion resistance due to its localized pitting corrosion behavior for both Ni-P and CrN layers. Through morphology observation, the nanolayered Ni-Al/CrN and Ni-P/CrN coatings maintained a solid integrity after corrosion test. The combination of Ni-P and CrN in a nanolayered coating structure to promote the corrosion resistance was demonstrated.

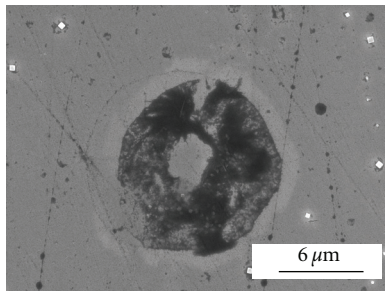

(a)

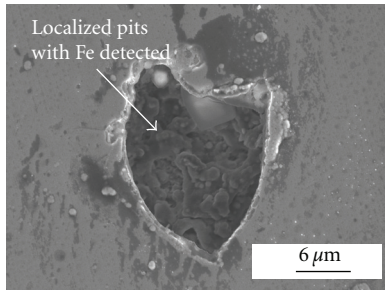

(b)

Figure 6: The SEM surface images of corroded regions of (a) NiP/CrN, (b) NiAl/CrN nanolayered coatings on stainless steel substrates.

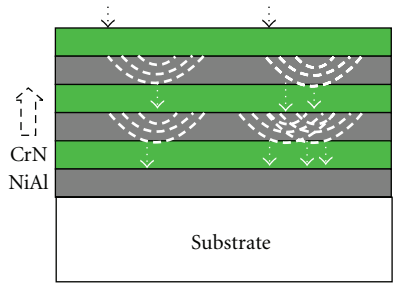

(a)

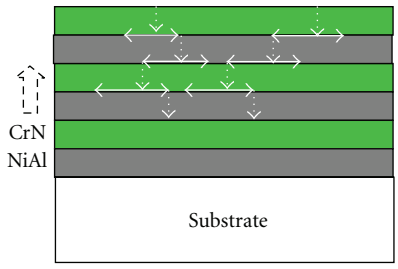

(b)

Figure 7: The schematic diagram of corrosion mechanism with (a) NiAl/CrN and (b) NiP/CrN nanolayered coatings.

Acknowledgment

This work is supported by the National Science Council, Taiwan, under Contracts nos. NSC-97-2221-E-239-008 and NSC 98-2221-E- 239-009-MY3.

References

[1] S.-K. Tien, J.-G. Duh, and J.-W. Lee, "Oxidation behavior of sputtered CrN/AlN multilayer coatings during heat treatment," *Surface and Coatings Technology*, vol. 201, no. 9–11, pp. 5138–5142, 2007.

[2] Y.-Z. Tsai and J.-G. Duh, "Thermal stability and microstructure characterization of CrN/WN multilayer coatings fabricated by ion-beam assisted deposition," *Surface and Coatings Technology*, vol. 200, no. 5-6, pp. 1683–1689, 2005.

[3] P. C. Yashar and W. D. Sproul, "Nanometer scale multilayered hard coatings," *Vacuum*, vol. 55, no. 3, pp. 179–190, 1999.

[4] M.-S. Wong, G.-Y. Hsiao, and S.-Y. Yang, "Preparation and characterization of AlN/ZrN and AlN/TiN nanolaminate coatings," *Surface and Coatings Technology*, vol. 133-134, pp. 160–165, 2000.

[5] D. C. Cameron, R. Aimo, Z. H. Wang, and K. A. Pischow, "Structural variations in CrN/NbN superlattices," *Surface and Coatings Technology*, vol. 142-144, pp. 567–572, 2001.

[6] I. Milošev, H.-H. Strehblow, and B. Navinšek, "XPS in the study of high-temperature oxidation of CrN and TiN hard coatings," *Surface and Coatings Technology*, vol. 74-75, no. 2, pp. 897–902, 1995.

[7] J.-N. Tu, J.-G. Duh, and S.-Y. Tsai, "Morphology, mechanical properties, and oxidation behavior of reactively sputtered Cr-N films," *Surface and Coatings Technology*, vol. 133-134, pp. 181–185, 2000.

[8] A. Kawashima, H. Habazaki, and K. Hashimoto, "Highly corrosion-resistant Ni-based bulk amorphous alloys," *Materials Science and Engineering A*, vol. 304-306, no. 1-2, pp. 753–757, 2001.

[9] G. Lu and G. Zangari, "Corrosion resistance of ternary Ni-P based alloys in sulfuric acid solutions," *Electrochimica Acta*, vol. 47, no. 18, pp. 2969–2979, 2002.

[10] J. G. González-Rodriguez, J. C. Colín, S. Serna, B. Campillo, and J. L. Albarran, "Effect of macroalloying with Cu on the corrosion resistance of rapidly solidified NiAl intermetallic in 0.5 M H_2SO_4," *Materials Science and Engineering A*, vol. 448, no. 1-2, pp. 158–164, 2007.

[11] F.-B. Wu, J.-J. Li, and J.-G. Duh, "Evaluation of the mechanical properties and tribological behavior of the CrN coating deposited on mild steel modified with electroless Ni interlayer," *Thin Solid Films*, vol. 377-378, pp. 354–359, 2000.

[12] J.-S. Chen, J.-G. Duh, and F.-B. Wu, "Microhardness and corrosion behavior in CrN/electroless Ni/mild steel complex coating," *Surface and Coatings Technology*, vol. 150, no. 2-3, pp. 239–245, 2002.

[13] F.-B. Wu and J.-G. Duh, "Scratch behavior and in situ acoustic emission analysis of PVD chromium nitride coatings on mild steel with electroless nickel interlayers," *Surface and Coatings Technology*, vol. 162, no. 1, pp. 106–112, 2003.

[14] Q. Yang and L. R. Zhao, "Thermal stability of polycrystalline TiN/CrN superlattice coatings," *Journal of Vacuum Science and Technology A*, vol. 21, no. 3, pp. 558–562, 2003.

[15] A. Bukaluk, "Auger electron spectroscopy investigations of the effect of degradation of depth resolution and its influence on the interdiffusion data in thin film Au/Ag, Cu/Ag, Pd/Au and Pd/Cu multilayer structures," *Applied Surface Science*, vol. 175-176, pp. 790–796, 2001.

[16] A. Bukaluk, "Influence of depth resolution on the interdiffusion data in thin film bilayer and multilayer Ag/Pd structures," *Vacuum*, vol. 63, no. 1-2, pp. 119–126, 2001.

[17] M. Ürgen and A. F. Çakir, "The effect of heating on corrosion behavior of TiN- and CrN-coated steels," *Surface and Coatings Technology*, vol. 96, no. 2-3, pp. 236–244, 1997.